Fluid motion of monomolecular films in a channel flow geometry

H. A. Stone[a)]
Division of Applied Sciences, Harvard University, Cambridge, Massachusetts 02138

(Received 26 August 1994; accepted 9 August 1995)

Surface pressure-driven flow of a monolayer in a channel flow geometry is studied and exact representations for the monolayer and subphase velocity fields are given in terms of solutions involving dual integral equations. The monolayer velocity profiles are examined as a function of the viscosity contrast between the monolayer and the subphase and the effects of a finite depth sublayer are investigated also. The calculated velocity profiles may prove useful for determining the effective surface viscosity of monolayer films from comparable experimental measurements. © *1995 American Institute of Physics.*

I. INTRODUCTION

The fluid dynamical properties of monomolecular films and other fluid-like membranes at the air-water interface, or other fluid-fluid interfaces, have been the subject of both classical analyses as well as many recent experimental and theoretical studies. An excellent survey of the field is provided by Edwards *et al.*[1] Modern investigations of monolayers and bilayers have been motivated by both biological and materials applications and have been accompanied by an improved understanding of the physicochemical properties of these systems.[2] In particular, it is known that as the surface pressure is varied the structure of the monolayer may change with domains of higher molecular concentration existing in a continuous phase of lower molecular concentration. Hydrodynamic issues that are discussed in recent research include measuring the effective viscosity of surface films,[3,4] calculating the diffusion coefficient for membrane-bound proteins,[5–8] and determining the shape changes of lipid domains imbedded in monolayers.[9,10] In all of these studies the thin molecular surface film is modelled as a distinct Newtonian fluid layer with a flow resistance characterized by an effective viscosity.

An important, and unusual, feature of the flow properties of these surface films is that a significant, and in some cases dominant, contribution to the resistance experienced by a surface motion is provided by the subphase liquid (usually water). The earliest method for measuring the surface, or effective, viscosity of a distinct monomolecular film utilized the so-called canal surface viscometer[1,11] whose fluid flow behavior, accounting for coupling of the surface film and the subphase, was first analyzed by Harkins and Kirkwood[12] with details provided by Hansen.[13] In this paper we discuss a modern relative of these earlier studies. In particular, we present an exact solution for the velocity fields in the monolayer and subphase liquids for a recent laboratory experiment described by Schwartz *et al.*,[4] which involves pressure-driven channel flow of a monolayer over a subphase of finite depth and infinite horizontal extent. We suggest that this analytical solution may be used to determine the effective viscosity of the film, the subphase layer thickness, or the viscosity of the subphase liquid. As we shall see, however, for typical material properties and experimental configurations the subphase resistance is dominant and the extraction of the surface viscosity from experimental measurements is very sensitive to small variations in the data.

In the classical canal surface viscometer, there is a narrow fluid-filled channel on which a monolayer is floated and forced to flow by applying a surface pressure gradient.[1,11] Experimental measurements verifying the original theory of Harkins and Kirkwood were apparently first reported only recently by Sacchetti *et al.*[3] An alternative, boundary-driven version of the canal viscometer, utilizing a Couette arrangement, was analyzed and implemented by Mannheimer and Schecter[14] and is discussed further by Edwards *et al.*[1]

Using a variant of the original canal surface viscometer, Schwartz *et al.*[4] recently reported experimental measurements for the monolayer velocity profiles in the channel flow

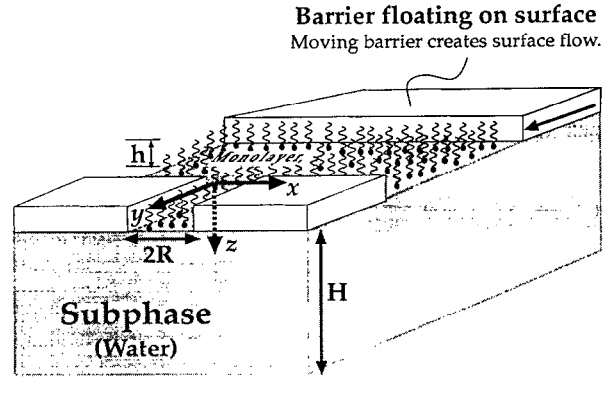

FIG. 1. The channel flow experiment of Schwartz *et al.*[4] A monolayer that exists in the two-phase (liquid-expanded/liquid-condensed) region is forced by a surface pressure gradient to flow through a channel that lies on the surface. The subphase is therefore forced to move also.

a)Phone: (617) 495-3599; fax: (617) 495-9837; e-mail: has@stokes.harvard.edu

 1070-6631/95/7(12)/2931/7/$6.00

of liquid monomolecular films set into motion by applying a surface pressure gradient. Unlike the original canal surface viscometer, the subphase liquid is not confined to a narrow channel but rather is contained in a trough much wider than the surface channel (see figure 1). The fluid motion in this flow apparatus is the subject of this paper. It should also be noted that in the experiments of Schwartz *et al.* the monolayer existed in the two-phase region with one phase broken into a large number of separate domains each of which is surrounded by the second continuous phase. The monolayer flow was observed by simply following the motion of one of the domains. Thus, for this phase-separated state we treat the monolayer as a distinct fluid phase with an effective Newtonian viscosity and assume a surface pressure-driven flow with constant pressure gradient (throughout the channel the surface pressure is such that the system remains in the two-phase region).

The simplest description of the fluid dynamics of a surface film treats it as a Newtonian fluid with a surface viscosity $\mu_s = \mu_m h$, where μ_m is the equivalent shear viscosity of the bulk membrane material and h is the (average) film thickness. When the surface film overlays a Newtonian fluid of viscosity μ, motions in the two layers are coupled and may be characterized by the dimensionless ratio

$$\Lambda = \frac{\mu R}{\mu_m h} = \frac{\mu R}{\mu_s}. \tag{1}$$

Here R is the characteristic length scale of the flow which is simply the channel width for the canal surface experiments. Schwartz *et al.*[4] demonstrate that the observed unidirectional surface pressure-driven monolayer velocity profiles, $v_m(x)$, for the apparatus shown in Figure 1, agree with a theoretical calculation based upon the limit that the drag provided by the subphase liquid exerts the dominant resistance to flow, $\Lambda \gg 1$:

$$v_m(x) \propto \sqrt{1-\left(\frac{x}{R}\right)^2}. \tag{2}$$

This elliptic velocity profile is broader and blunter than the parabolic Poiseuille profile which would be otherwise expected if the pressure-driven monolayer motion were independent of the subphase. This example clearly illustrates the significant dynamical influence of the fluid surrounding the membrane. The hydrodynamic influence of the subphase fluid had been discussed previously by Saffman[5] and Hughes *et al.*[6] in studies of the Brownian motion of protein molecules confined to bilayers, by Klinger and McConnell[15] in a study of the Brownian motion of lipid domains at the air-water interface, and by Stone and McConnell[9] in a study of shape instabilities of lipid domains.

In this paper we analyze as a function of the viscosity ratio parameter Λ the velocity fields for the channel flow apparatus shown in Figure 1. In Sec. II the governing equations for the subphase and surface monolayer are presented. The unidirectional velocity fields are represented using Fourier cosine integrals. A system of dual integral equations is derived, recast into a form involving Bessel functions kernels, and solved numerically. Thus, the velocity fields throughout the system are established. A simple analytical result valid for thin sublayers is given in Sec. III. In Sec. IV, the monolayer velocity profiles are studied as a function of the dimensionless subphase depth and Λ. Finally, in Sec. V some implications for laboratory experiments are discussed.

II. PROBLEM STATEMENT AND SOLUTION

Consider the channel flow geometry illustrated in Figure 1. In the experiments described by Schwartz *et al.*[4] the channel was about 1 cm in length and 300 μm in width. A monolayer resided on the surface of a water layer which was 3–4 mm in depth. The monolayer existed in the so-called liquid expanded–liquid condensed region so that the surface film actually consisted of domains of higher surfactant concentration (liquid condensed) in a continuum of lower surfactant concentration (liquid expanded). The monomolecular film was forced by a surface pressure gradient (magnitude less than 10^{-3} mN/cm) to flow slowly; typical velocities were smaller than $u_c = O(200-300)\,\mu$m/sec. The surface velocity profiles measured by Schwartz *et al.* were independent of the area fraction of the liquid condensed domains.

Denote the cross-channel direction as x, the axial channel direction as y, and the vertical direction into the subphase as z. The channel width is denoted by $2R$ and the subphase, with depth H, is assumed to be unbounded in the x-direction. In the classical canal apparatus geometries the channel boundaries extended throughout the entire depth of the subphase. The viscosity of the (Newtonian) surface film is denoted μ_m, while the shear viscosity of the subphase liquid is denoted μ with the associated kinematic viscosity denoted ν. Motion of the surface film and subphase are coupled owing to viscous stresses exerted across the interface. The combined surface pressure-driven fluid motion is thus somewhat more complicated than the textbook examples of single-phase Poiseuille flow in a pipe or channel, which is obtained here in the limit of vanishing subphase viscosity. Nevertheless, as we shall now see, a relatively simple description of the entire flow field is possible.

A. Reduction to dual integral equations

The governing equations for the subphase fluid are the Navier-Stokes equations while the planar monolayer is described by a modified version of the Navier-Stokes equations which accounts for the viscous coupling of the surface film and subphase.[5,12] Away from the channel entrance and exit, we assume that the surface pressure gradient is constant in the y-direction and that the flow is steady and unidirectional. Thus, we seek a surface layer flow $\mathbf{u}_m(\mathbf{x}) = v_m(x)\mathbf{e}_y$ and a unidirectional two-dimensional sublayer flow $\mathbf{u}(\mathbf{x}) = v(x,z)\mathbf{e}_y$ (a subscript m is used to distinguish monolayer properties). Consequently, the nonlinear convective terms in the equations of motion are identically zero and the solution we construct below is therefore an exact solution to the Navier-Stokes equations for the given boundary forcings. For possibly more complicated surface film motions, we note that the Reynolds number characterizing the flow is small, $u_c R/\nu = O(10^{-2})$, so that viscous effects dominate everywhere and the linear equations solved here are the appropriate starting point.

We begin with the sublayer flow which is surface driven and invariant in the y-direction, hence satisfies $\nabla^2 v = 0$. As there is a plane of symmetry $v(x,z) = v(-x,z)$, and the sublayer is unbounded in the x-direction, a Fourier cosine representation of the velocity field is appropriate. In order to satisfy the no-slip condition on the lower boundary $v(x,H) = 0$, we may take $v(x,z)$ to have the form

$$v(x,z) = \int_0^\infty A(k) \frac{\sinh[k(H-z)]}{\cosh(kH)} \cos(kx)\, dk, \tag{3}$$

where $A(k)$ is to be determined. For $|x| > R$, the no-slip condition on the upper surface, $v(x,0) = 0$, must be satisfied.

The monolayer is assumed to remain planar and is modeled as a separate three-dimensional planar viscous Newtonian fluid phase of constant thickness h.[5] There is a constant surface pressure gradient, $dp_m/dy = (1/h)(d\Pi/dy) = \text{constant}$ where Π is the usual surface pressure measured in a Langmuir trough; for flow in the positive y-direction, $d\Pi/dy < 0$. The surface film experiences an additional body force owing to the molecular structure resisting out-of-plane distortions. This additional force, exerted by the subphase motion, is distributed throughout the layer thickness h and is equal to $(\mu/h)(\partial v/\partial z)|_{z=0}$. Thus, the membrane velocity $v_m(x)$ satisfies the ordinary differential equation

$$\mu_m \frac{d^2 v_m}{dx^2} - \frac{1}{h}\frac{d\Pi}{dy} + \frac{\mu}{h}\frac{\partial v}{\partial z}\Big|_{z=0} = 0 \quad \text{for } |x| < R. \tag{4}$$

The surface viscosity μ_s, which is often used to describe monolayers, is given in our notation as $\mu_s = \mu_m h$.

Continuity of velocity at the monolayer-subphase interface requires that

$$v_m(x) = v(x,0) = \int_0^\infty A(k)\tanh(kH)\cos(kx)\, dk. \tag{5}$$

Substituting (5) into (4) and using (3) to evaluate the additional surface force term we arrive at

$$\int_0^\infty A(k)\left[k^2 \mu_m \tanh(kH) + \frac{\mu k}{h}\right]\cos(kx)\, dk = -\frac{1}{h}\frac{d\Pi}{dy} \quad \text{for } |x| < R. \tag{6}$$

For $|x| > R$, no-slip on the upper apparatus boundary requires

$$\int_0^\infty A(k)\tanh(kH)\cos(kx)\, dk = 0 \quad \text{for } |x| > R. \tag{7}$$

We thus have a system of dual integral equations (6 and 7) for the unknown function $A(k)$. It is convenient to scale all lengths by R, let $\bar{x} = x/R$, $s = kR$ and define

$$A(k) = \bar{A}(s)\frac{R^3}{\mu_m h}\frac{d\Pi}{dy}. \tag{8}$$

Therefore, the function $\bar{A}(s)$ is defined in terms of the dual integral equations

$$\int_0^\infty \bar{A}(s)[s\tanh(sH/R) + \Lambda] s\cos(s\bar{x})\, ds = -1 \quad \text{for } |\bar{x}| < 1, \tag{9}$$

$$\int_0^\infty \bar{A}(s)\tanh(sH/R)\cos(s\bar{x})\, ds = 0 \quad \text{for } |\bar{x}| > 1, \tag{10}$$

where Λ is given by equation (1) and denotes an effective viscosity contrast between the surface layer and subphase.

The mathematical problem has been reduced to solving for $\bar{A}(s)$ from which the velocity profiles can be determined. The two dimensionless parameters that appear are Λ and H/R. Typical values of the material properties are $\mu = 10^{-2}$ gr/cm·sec and $\mu_s = 10^{-5} - 10^{-7}$ gr/sec, while $R \approx 150$ μm so that $\Lambda = O(10 - 10^3)$; for narrow channels $\Lambda = O(1)$ is possible.

B. Solution of the dual integral equations

Dual integral equations with trigonometric kernels are discussed by Sneddon[16] (Sec. 4.5). Here we have found it convenient to use an analytical approach due to Tranter.[17,18] To begin with, since

$$J_{-1/2}(s\bar{x}) = \sqrt{\frac{2}{\pi s\bar{x}}}\cos(s\bar{x}) \tag{11}$$

where $J_{-1/2}$ is the Bessel function, then (9) and (10) may be written

$$\int_0^\infty \bar{A}(s) s^{3/2}[s\tanh(sH/R) + \Lambda] J_{-1/2}(s\bar{x})\, ds = -\sqrt{\frac{2}{\pi\bar{x}}} \quad \text{for } |\bar{x}| < 1, \tag{12}$$

$$\int_0^\infty \bar{A}(s) s^{1/2}\tanh(sH/R) J_{-1/2}(s\bar{x})\, ds = 0 \quad \text{for } |\bar{x}| > 1. \tag{13}$$

Tranter[18] (Chapter 8) describes a straightforward procedure for constructing analytical solutions to this form of dual integral equations with Bessel function kernels. The solution method is motivated by the identity (the Weber-Schafheitlin discontinuous integral)

$$\int_0^\infty s^{1-\beta} J_{2m-(1/2)+\beta}(s) J_{-1/2}(s\bar{x})\, ds = 0 \quad \text{for } \bar{x} > 1 (\beta > 0), \tag{14}$$

which suggests that we may automatically satisfy equation (13) by representing the unknown function $\bar{A}(s)$ as the series

$$\bar{A}(s) s^{1/2}\tanh(sH/R) = s^{1-\beta}\sum_{m=0}^{\infty} a_m J_{2m-(1/2)+\beta}(s). \tag{15}$$

The constant β may be chosen later to simplify evaluation of integrals which appear below. Tranter's procedure is to substitute (15) into (12), multiply both sides by $\bar{x}^{1/2}(1-\bar{x}^2)^{\beta-1}\mathcal{F}_n(\beta - \frac{1}{2}, \frac{1}{2}; \bar{x}^2)$, where $\mathcal{F}_n$ is a Jacobi polynomial, integrate both sides from $\bar{x} = 0$ to 1, and then use the two identities (take $\nu = -1/2$):

$$s^{-\beta}J_{2n+\nu+\beta}(s)$$

$$=\frac{\Gamma(\nu+n+1)}{2^{\beta-1}\Gamma(\nu+1)\Gamma(n+\beta)}\int_0^1 \bar{x}^{\nu+1}(1-\bar{x}^2)^{\beta-1}$$

$$\times \mathscr{F}_n(\beta+\nu,\nu+1;s^2)J_\nu(s\bar{x})d\bar{x} \tag{16}$$

and

$$\int_0^1 \bar{x}^{2\nu+1}(1-\bar{x}^2)^{\beta-1}\mathscr{F}_n(\beta+\nu,\nu+1;\bar{x}^2)d\bar{x}$$

$$=\frac{\Gamma(\nu+1)\Gamma(\beta)}{2\Gamma(\nu+\beta+1)}\delta_{0n}. \tag{17}$$

We thus arrive at an infinite linear system of equations for the constants a_m:

$$\sum_{m=0}^{\infty} a_m\int_0^\infty G(s;\Lambda,H/R)s^{1-2\beta}J_{2m-(1/2)+\beta}(s)$$

$$\times J_{2n-(1/2)+\beta}(s)ds=-\frac{2^{(1/2)-\beta}\delta_{0n}}{\Gamma(\beta+(1/2))} \quad n=0,1,2,\ldots \tag{18}$$

where

$$G(s;\Lambda,H/R)=s(s+\Lambda\coth(sH/R)). \tag{19}$$

The constant β is chosen in order to guarantee convergence of the integrals in (18) and so we take $\beta=2$ for the numerical calculations reported here. All numerical calculations are performed in double precision. The integrals in (18), which involve products of Bessel functions, are evaluated using the numerical routines developed and described by Lucas.[19] The a_m are then determined by truncating (18) at N terms and solving the $N\times N$ linear system using the IMSL routine DLSARG. Typically $N=11$ terms in the equations are retained; numerical calculations with more terms demonstrate that the results presented here are accurate to within a few percent. In the integration routines, the absolute and relative error bounds are set at 10^{-6} and 10^{-8}, respectively.

Once the a_m are determined, $A(k)$ is known from (8) and (15), and the velocity fields may be calculated using equations (3) and (5). For example, with $\beta=2$,

$$\frac{v_m(x)}{-\left(\frac{R^2}{\mu_m h}\right)\left(\frac{d\Pi}{dy}\right)}$$

$$=-\sum_{m=0}^{\infty} a_m\int_0^\infty s^{-3/2}J_{2m+(3/2)}(s)\cos(s\bar{x})ds$$

$$\text{for } |x|<1. \tag{20}$$

The centerline velocity $v_m(0)$ may be evaluated explicitly as (Gradshteyn and Ryzhik,[20] p. 684, equation 6.561.14)

$$\frac{v_m(0)}{-\left(\frac{R^2}{\mu_m h}\right)\left(\frac{d\Pi}{dy}\right)}=-\sum_{m=0}^{\infty} a_m\frac{\Gamma(m+(1/2))}{(m+1)!}, \tag{21}$$

where Γ is the Gamma function. Evaluation of the velocity fields, e.g. (20) with (11), also requires integrations which involve products of Bessel functions. Although some analytical simplification is possible in terms of a reduction to a series of hypergeometric functions, it is simpler numerically to evaluate the original integrals directly.

The limit of an infinitely deep subphase is obtained by letting $H/R\to\infty$ which corresponds to setting the hyperbolic tangent terms to unity. In practice, the effect of H/R is significant for $H/R<1$ as the numerical calculations in Sec. IV demonstrate.

III. THIN SUBLAYERS

In the thin sublayer limit, $H/R\ll 1$, we expect that the viscous coupling experienced by the surface film is given by assuming that the sublayer flow is very nearly a linear shear flow.[6] Thus, $\partial v/\partial z|_{z=0}\approx -v_m(x)/H$ and so equation (4) becomes

$$\mu_m\frac{d^2v_m}{dx^2}-\frac{\mu}{hH}v_m=\frac{1}{h}\frac{d\Pi}{dy}. \tag{22}$$

The solution to this equation which satisfies the boundary conditions is

$$v_m(x)=-\frac{H}{\mu}\frac{d\Pi}{dy}\left[1-\frac{\cosh\sqrt{\frac{\Lambda R}{H}}\frac{x}{R}}{\cosh\sqrt{\frac{\Lambda R}{H}}}\right] \quad \left(\frac{H}{R}\ll 1\right). \tag{23}$$

We shall see in Sec. IV by direct comparison with the exact solution that in practice the above approximation is quite useful provided $H/R<1$.

IV. RESULTS

We begin by noting that two simple limits exist, as mentioned by Schwartz *et al.*[4] For the case that $\Lambda\ll 1$, the monolayer provides the primary resistance to flow and the velocity profile is clearly a two-dimensional Poiseuille channel flow:

$$\frac{v_m(x)}{-\frac{R^2}{\mu_m h}\frac{d\Pi}{dy}}=1-\left(\frac{x}{R}\right)^2 \quad (\Lambda\ll 1). \tag{24}$$

On the other hand, for $\Lambda\gg 1$, the subphase provides the dominant resistance to flow and the velocity profile has the distinctive elliptic form given explicitly by

$$\frac{v_m(x)}{-\frac{R}{\mu}\frac{d\Pi}{dy}}=\sqrt{1-\left(\frac{x}{R}\right)^2} \quad (\Lambda\gg 1). \tag{25}$$

A derivation of this result utilizing the dual integral equation approach of Sec. II is given in the Appendix. Schwartz *et al.* present experimental results that are in excellent agreement with (25). We also note that in the limit $\Lambda\gg 1$, the boundary value problem reduces to $\nabla^2 v=0$ with $\partial v/\partial z=$constant on $z=0,|x|<1$ with $v=0$ on $z=0,|x|>1$. This problem is equivalent to that of potential (ideal) fluid flow through a slit which has been studied by Hasimoto[21] and for which the

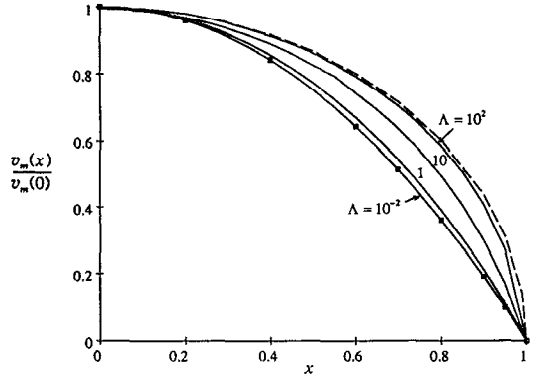

FIG. 2. Monolayer velocity profiles as a function of Λ; $H/R = 100$. The square symbols correspond to the Poiseuille profile, equation (24), and the dashed curve is the square root profile, equation (25).

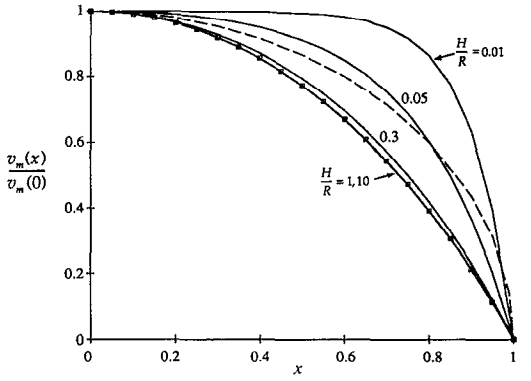

FIG. 4. Monolayer velocity profile as a function of H/R; $\Lambda = 1$. The dashed curve is the square root velocity profile representative of the limit $\Lambda \gg 1$. The square symbols are the predictions of the thin layer analysis (23) for $H/R = 1$.

velocity profile in the plane of the slit corresponds to (25). (We thank Professor A. Acrivos for pointing out this analogy.)

In figure 2 we show the monolayer velocity profiles $v_m(x)$ as a function of Λ for $H/R = 100$ which corresponds to a very deep subphase. Each of the curves is normalized with respect to the centerline velocity $v_m(0)$. Also shown in the figure are the limits of a two-dimensional Poiseuille channel flow, equation (24), denoted by the square symbols, and the square root velocity profile, equation (25), represented by the dashed curve. As Λ increases we span behavior from the Poiseuille profile to the square root profile. The effect of increasing the viscosity of the subphase, i.e. larger values of Λ, leads to a broadening and blunting of the velocity profile. The results indicate that at $x = 0.75$ the velocity, relative to the centerline velocity, is increased by nearly 50 percent as Λ increases from 10^{-2} to 10^2.

An effect of increasing Λ for a fixed value of the subphase depth and applied surface pressure gradient $d\Pi/dy$ is to substantially decrease the magnitudes of the monolayer velocities. This effect is shown by the solid curves in figure 3 where the centerline velocity $v_m(0)$ is given as a function of Λ and H/R. The dashed curve is a prediction from the thin sublayer analysis (23). As Λ increases from 1 to 10^2, the centerline velocity drops by a comparable factor of 100, which clearly illustrates the large and dominant resistance offered by the subphase; for $\Lambda > O(1)$ the velocities decrease as $O(\Lambda^{-1})$. We also observe that the effect of varying the depth of the sublayer becomes noticeable when $H/R \lesssim 5$. For $\Lambda > O(1)$, decreasing H/R from 1.0 to 0.3 decreases the centerline velocity by more than a factor of two. For even thinner sublayers the velocities decrease as $O(H/R)$ owing to the large viscous stresses in the thin subphase. As illustrated in figure 3 by the dashed curve, the simple prediction given by (23) is in excellent agreement with the numerical results for $H/R = 0.3$ though for $\Lambda > 10$ and $H/R = 1$ (not shown), the thin layer approximation deviates by more than 25% from the numerical results. For $\Lambda < O(10^{-1})$, changing H/R has only a small effect for the range of values considered since the monolayer properties control the resistance.

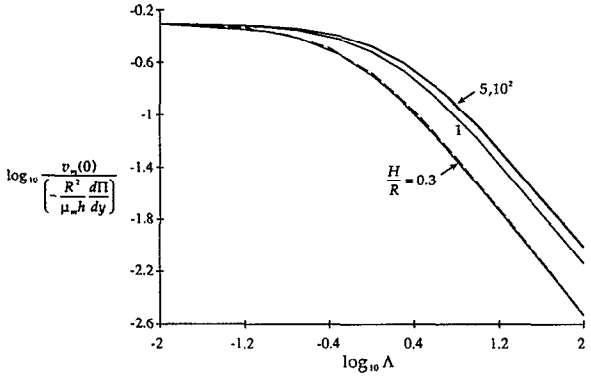

FIG. 3. Centerline velocity as a function of Λ and H/R. The dashed curve is calculated using (23).

In figure 4 we investigate the effect on the monolayer velocity profile caused by changing the sublayer depth for fixed material properties ($\Lambda = 1$). For $H/R > 1$, the velocity profile is practically unchanged. As H/R decreases below unity, the velocity profile broadens (and the typical speeds decrease as illustrated in figure 3). The effect of decreasing H/R is not equivalent, however, to simply increasing Λ since the velocity profile is not identical to the square root velocity profile, equation (25), obtained in the limit $\Lambda \gg 1$ and shown as the dashed curve in the figure. In fact, for $H/R \ll 1$, the velocity profile becomes almost uniform across the channel and the centerline velocity (scaled by $(d\Pi/dy)R^2/\mu_m h$) has magnitude $O(\Lambda^{-1}H/R)$ as may be obtained from (23). Also, in figure 4 the detailed predictions of the thin layer analysis (23) are shown for $H/R = 1$ by the square symbols and are in excellent agreement with the numerical results. This agreement becomes less good as Λ increases since more of the sublayer fluid, away from the channel region, flows owing to viscous stresses.

V. DISCUSSION

The principal contribution of this research is an exact solution for the unidirectional velocity fields consistent with

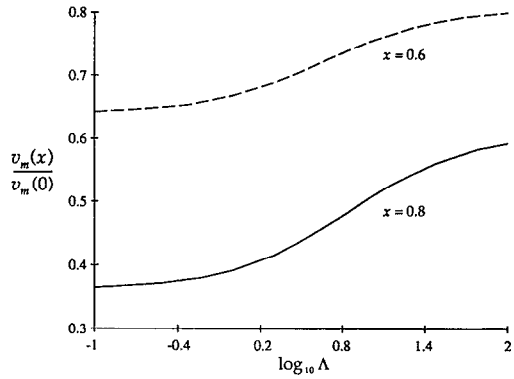

FIG. 5. The normalized monolayer velocity at $x=0.8$ (solid curve) and at $x=0.6$ (dashed curve) as a function of Λ; $H/R=1$.

the channel flow apparatus described by Schwartz *et al.*[4] It is apparent from the numerical results presented in Sec. IV that a parabolic monolayer velocity profile is obtained provided $\Lambda \lesssim O(10^{-1})$ and $H/R \gtrsim O(1)$. The square root velocity profile, equation (25), characteristic of the dominant resistance originating in the subphase is expected for $\Lambda > O(10^2)$ for $H/R \gtrsim O(1)$. For thin sublayers, $H/R < 0.05$, the monolayer velocity profile becomes more uniform and, at least in a qualitative sense, behaves similar to a more viscous subphase.

Finally, we should like to address the use of these results for determining the effective surface viscosity of a monolayer from a series of experimental measurements of the surface velocity profile. The numerical results suggest that such a measurement is susceptible to small measurement errors for large Λ since there is little difference between the square root profile (25), which is independent of μ_s, and the results for $\Lambda > O(10^2)$, at least for $H/R > 1$ (e.g. figure 2). For such cases only an order-of-magnitude estimate of the surface viscosity will be possible.

However, for $\Lambda < 10$, it seems possible to determine a reliable value for μ_s provided the subphase viscosity μ and channel width R are known and $H/R > 1$. For example, the velocity, normalized to the centerline velocity, at a given x-position, is a unique function of Λ for a given H/R. In figure 5, we thus plot with a solid curve $v_m(0.8)/v_m(0)$ versus Λ for $H/R=1$. For comparison, $v_m(0.6)/v_m(0)$ is shown with a dashed curve. Results calculated for $H/R=100$ differ by about two percent.

One way to use the numerical results is to measure $v_m(0.8)/v_m(0)$ and obtain from the curve in Figure 5 the corresponding value of Λ (the normalized velocity at any other x-location could be measured instead; the author will happily make available the computer programs which perform the desired calculations). The surface viscosity follows from $\mu_s = \mu_m h = \mu R/\Lambda$. As an example, we can examine the data reported by Schwartz *et al.*[4] who measured $v_m(0.8)/v_m(0)=0.60$, which corresponds to $\Lambda=200$. Although this value of Λ is in the range where small measurement uncertainty produces significant errors in μ_s, we may nonetheless estimate $\mu_s = 8\times10^{-7}$ gm/sec, which is about 10 times smaller than the value estimated by Schwartz *et al.*

ACKNOWLEDGMENTS

I am thankful to Harden McConnell for introducing me to this fascinating subject and for bringing the paper by Evans and Sackmann to my attention, Steven Lucas for making available to me programs to evaluate infinite integrals with kernels involving products of Bessel functions, John Tanzosh for helpful conversations concerning 'Tranter's method', Bill Foster for providing me with a preprint of the paper by Schwartz *et al.*, Peter Pershan for bringing the paper by Sacchetti *et al.* to my attention, Dan Schwartz for helpful comments, Selena Rose for assistance with figure 1, and Andy Acrivos for pointing out the analogy to the potential flow in a slit geometry. Financial support from NSF-Presidential Young Investigator Award CTS-8957043 is gratefully acknowledged.

APPENDIX: THE LIMIT $\Lambda \gg 1$

In the limit $\Lambda \gg 1$, the subphase exerts the dominant resistance to motion of the monolayer. Thus, at leading order, in equation (4) we neglect the $\mu_m \nabla^2 \mathbf{u}_m$ term. We are thus dealing with a singular perturbation problem which gives rise to narrow boundary layers[22] $O(R\Lambda^{-2/3})$ in the neighborhood of the channel boundaries at $x=\pm R$. We will, however, be satisfied with deriving the leading order solution valid throughout the majority of the channel. Also, we will only consider the deep channel limit $H/R \to \infty$.

Neglecting the monolayers' viscous contribution and taking $H/R \to \infty$, the Fourier cosine transform solution outlined in Sec. II B, equations (12)–(13), leads to the dual integral equations

$$\int_0^\infty \bar{A}(s) s^{3/2} J_{-1/2}(s\bar{x})\,ds = -\frac{1}{\Lambda}\sqrt{\frac{2}{\pi\bar{x}}} \quad \text{for } |\bar{x}|<1, \tag{A1}$$

$$\int_0^\infty \bar{A}(s) s^{1/2} J_{-1/2}(s\bar{x})\,ds = 0 \quad \text{for } |\bar{x}|>1. \tag{A2}$$

We seek a solution

$$\bar{A}(s) = s^{(1/2)-\beta} \sum_{m=0}^{\infty} a_m J_{2m-(1/2)+\beta}(s) \quad (\beta>0), \tag{A3}$$

and by following the steps described in Sec. II B obtain the linear system of equations

$$\sum_{m=0}^{\infty} a_m \int_0^\infty s^{2-2\beta} J_{2m-(1/2)+\beta}(s) J_{2n-(1/2)+\beta}(s)\,ds = -\frac{2^{(1/2)-\beta}\delta_{0n}}{\Lambda\Gamma(\beta+1/2)} \quad n=0,1,2. \tag{A4}$$

If we choose $\beta=3/2$ the integral on the left may be evaluated exactly[18]

$$\int_0^\infty s^{-1} J_{2m+1}(s) J_{2n+1}(s)\,ds = (4n+2)^{-1}\delta_{mn}, \tag{A5}$$

and so we find

$$a_0 = -\frac{1}{\Lambda} \quad \text{and} \quad a_n \equiv 0 \quad \text{for } n \geq 1. \tag{A6}$$

Finally, evaluating the velocity field we have (see for example Watson[23])

$$\frac{v_m(x)}{-\frac{R^2}{\mu_m h}\frac{d\Pi}{dy}} = -\sum_{m=0}^{\infty} a_m \int_0^{\infty} s^{-1} J_{2m+1}(s) \times \cos(s\bar{x})\,ds \quad \text{for } |x|<1, \tag{A7}$$

$$= -\sum_{m=0}^{\infty} a_m \frac{1}{2m+1}\cos((2m+1)\sin^{-1}\bar{x}) \tag{A8}$$

$$= -a_0\sqrt{1-\bar{x}^2} \tag{A9}$$

or

$$\frac{v_m(x)}{-\frac{R}{\mu}\frac{d\Pi}{dy}} = \sqrt{1-\left(\frac{x}{R}\right)^2} \tag{A10}$$

as given in equation (25) and stated by Schwartz *et al.*[4] As mentioned earlier this mathematical problem corresponds to the potential flow through a slit geometry whose solution using complex variable methods is summarized by Hasimoto.[21]

Finally, we note that it is also possible to argue that for $\Lambda \ll 1$ the dual integral equation formulation leads to the Poiseuille profile (24). Set $\Lambda=0$ in equation (18) and consider the deep subphase limit $H/R \to \infty$. Taking $\beta=2$ the integrals can be evaluated analytically and the velocity profile can be written as a hypergeometric series which truncates after the second term to give a Poiseuille profile.

[1] D. A. Edwards, H. Brenner, and D. T. Wasan, *Interfacial Transport Processes and Rheology* (Butterworth-Heinemann, Boston, 1991).

[2] H. M. McConnell, "Structures and transitions in lipid monolayers at the air–water interface," Annu. Rev. Phys. Chem. **42**, 171 (1991).

[3] M. Sacchetti, H. Yu, and G. Zografi, "Hydrodynamic coupling of monolayers with subphase," J. Chem. Phys. **99**, 563 (1993).

[4] D. Schwartz, C. M. Knobler, and R. Bruinsma, "Direct observation of Langmuir monolayer flow through a channel," Phys. Rev. Lett. **73**, 2841 (1994).

[5] P. G. Saffman, "Brownian motion in thin sheets of viscous fluid," J. Fluid Mech. **73**, 593 (1976).

[6] E. Evans and E. Sackmann, "Translational and rotational drag coefficients for a disk moving in a liquid membrane associated with a rigid substrate," J. Fluid Mech. **194**, 553 (1988).

[7] B. D. Hughes, B. A. Pailthorpe, and L. R. White, "The translational and rotational drag on a cylinder moving in a membrane," J. Fluid Mech. **110**, 349 (1981).

[8] S. J. Bussell, D. L. Koch, and D. A. Hammer, "The resistivity and mobility functions for a model system of two equal-sized proteins in a lipid bilayer," J. Fluid Mech. **243**, 679 (1992).

[9] H. A. Stone and H. M. McConnell, "Hydrodynamics of quantized shape transitions of lipid domains," Proc. R. Soc. London Ser. A **448**, 97 (1994).

[10] R. E. Goldstein and D. P. Jackson, "Domain shape relaxation and the spectrum of thermal fluctuations in Langmuir monolayers," J. Phys. Chem. **98**, 9626 (1994).

[11] F. C. Goodrich, in *Progress in Surface and Membrane Science,* edited by J. F. Danielli, M. D. Rosenberg, and D. A. Cadenhead (Academic, New York, 1973), Vol. 7, p. 151.

[12] W. D. Harkins and J. G. Kirkwood, "The viscosity of monolayers: Theory of the surface slit viscosimeter," J. Chem. Phys. **6**, 53 (1938).

[13] R. S. Hansen, "Film and substrate flow in surface channels," J. Phys. Chem. **63**, 637 (1959).

[14] R. J. Mannheimer and R. S. Schechter, "An improved apparatus and analysis for surface rheological measurements," J. Coll. Int. Sci. **32**, 195 (1970).

[15] J. F. Klinger and H. M. McConnell, "Brownian motion and fluid mechanics of lipid monolayer domains," J. Phys. Chem. **97**, 6096 (1993).

[16] I. N. Sneddon, *Mixed Boundary Value Problems in Potential Theory* (Wiley, New York, 1966).

[17] C. J. Tranter, "A further note on dual integral equations and an application to the diffraction of electromagnetic waves," Q. J. Mech. Appl. Math. **7**, 317 (1954).

[18] C. J. Tranter, *Integral Transforms in Mathematical Physics* (Wiley, New York, 1966).

[19] S. K. Lucas, "Evaluating infinite integrals involving products of Bessel functions of arbitrary order," to appear in J. Comput. Appl. Math. (1995).

[20] I. S. Gradshteyn and I. M. Ryzhik, *Tables of Integrals, Series and Products* (Academic, San Diego, 1965).

[21] H. Hasimoto, "On the flow of a viscous fluid past a thin screen at small Reynolds numbers," J. Phys. Soc. Jpn. **13**, 633 (1958).

[22] The neglect of the monolayer viscous stresses produces the surface velocity profile $v_m(x) \propto \sqrt{1-\bar{x}^2}$. Hence, the associated monolayer viscous stresses become large $O(\mu_m R^{-2}(1-\bar{x}^2)^{-3/2})$ for $\bar{x} \to 1$. Thus, there must exist a boundary layer with typical thickness $R\delta$, $\delta \ll 1$, near $\bar{x}=1$ such that the stresses remain comparable to those from the sublayer flow. Retaining all dimensions and referring to equation (4): $O(\mu_m R^{-2}\delta^{-3/2}) \approx O(\mu(hR)^{-1})$ so that the boundary layer has thickness $R\delta \approx (\mu_s/\mu)^{2/3}R^{1/3}$ which was indicated by Schwartz *et al.*[4]

[23] G. N. Watson, *Treatise on the Theory of Bessel Functions* (Cambridge University Press, Cambridge, 1945), p. 405.